

GEOMETRICALLY EXACT MODEL OF CANTILEVER BEAM UNDERGOING LARGE DEFLECTION AND LINEARIZED DYNAMICS CHARACTERIZATION

Changyun Yang[1], Ran Zhao[1], Yingsong Gu[1,2] & Zhichun Yang[1,2]

[1]School of Aeronautics, Northwestern Polytechnical University, Xi'an, Shaanxi 710072, China
[2]National Key Laboratory of Strength and Structural Integrity, Xi'an 710072, PR China

Abstract

Nonlinear beam theories are widely used to study the mechanical behavior of high-aspect-ratio flexible wings, helicopter rotor blades, deep-sea risers and pipelines. However, present theoretical models usually introduce some simplifications in the research process. For example, the higher-order terms of are neglected when using Green's strain to characterize the geometric nonlinear relationship, using the axial coordinates of the beam to approximately replace the arc-length coordinates, or simplifying the structure stress or strain when using the arc-length method to characterize the structural deformation. These treatments may cause the theoretical analysis results to deviate from the finite element simulation or experimental results. In this paper, the kinetic energy and potential energy of Euler-Bernoulli beam undergoing large deformation are accurately described with arc length and curvature coordinates. The rotation angle of the beam is discretized by Galerkin method, and the control equation of the cantilever beam structure with applied load is derived based on Lagrange method. The static large deformation of the beam structure subjected to external loads is solved, and the modal frequencies in the resulting deformed state are obtained. The calculation results of the present model agree well with those by the finite element simulation and experiment, which indicates that the geometrically exact inextensible model based on curvature and arc length coordinates has high accuracy. Moreover, the present model successfully captures typical nonlinear dynamic phenomena such as stiffness hardening and hysteresis in the frequency response.

Keywords: nonlinear beam, inextensible, geometrically exact, large deformation, nonlinear modal analysis

1. Introduction

The development of geometrically exact beam theories has been a major achievement in nonlinear mechanics. Starting from the seminal works of Reissner[1-3] and Simo[4-6], the finite‐strain beam theory provides a rigorous framework for structures undergoing large deflections and rotations. In this theory, the beam configuration is described in terms of the position of the centroid line and the orientation of the cross‐section, leading to exact strain measures that satisfy objectivity and path‐independence[7, 8]. The finite element method (FEM) has been the primary numerical tool for implementing this theory, and it has proven highly accurate for static, dynamic, and aeroelastic problems[9-13].

Nevertheless, FEM solutions are typically obtained by time marching, which makes frequency‐domain analyses quite challenging, such as the harmonic balance method (HBM) for nonlinear modal characteristics analysis. On the other hand, semi−analytical methods like the Galerkin approach provide an effective approach for modeling order reduction that can be combined with perturbation methods, pseudo arc-length continuation method, and HBM[14-17]. However, when applied to nonlinear beam models, existing Galerkin formulations often introduce approximations that compromise model exactness. For instance, many semi−analytical studies use the axial coordinate instead of the arc length[18-22], employ truncated Green-Lagrange strain measures[23-25], or neglect higher‐order inertia couplings[26]. These simplifications are acceptable for small or

moderate rotations, but they fail when the beam undergoes extreme bending, such as tip rotations exceeding π/2.

A key concept that can bridge the gap between geometric exactness and semi−analytical efficiency is the inextensible beam assumption. For many slender structures, axial stretching be ignored for cantilever beams or free-free beams that are not subjected to significant axial forces[27-31]. Under this assumption, the axial displacement becomes a function of the lateral deflection, and the beam kinematics can be described solely by the arc length coordinate and the cross‑section rotation angle. Based on this, Fiori[32] provided a systematic review of geometrically exact beam theory using Lie group theory, with a specific focus on the theoretical framework under the inextensible assumption. Luongo and D' Annibale[33] established a nonlinear dynamic model of Beck's beam based the geometrically exact beam theory and inextensible assumption, and the Galerkin approach for the solution is provided. However, only one mode is retained and the high-order Taylor expansion terms of trigonometric function were ignored, which reduced the computational accuracy of the model.

The present work aims to develop a geometrically exact inextensible beam model for the Galerkin approach, without any simplification. In this study, all terms in the potential energy, kinetic energy and virtual work by loads are exactly expressed by arc length coordinates and rotation angle, and the rotation angle are discretized via the Galerkin method. By applying the Lagrangian equation, governing equation are derived as a semi-analytical formula suitable for numerical solution. By calculating static deformation, modal analysis, and dynamic response, and comparing them with numerical simulations, the accuracy of the model established in this paper is verified. Furthermore, the influence of excitation amplitude on the hysteresis phenomena is investigated based on the present model.

2. Methodology

2.1 Governing equation

In conventional nonlinear beam theories, the structural configuration is commonly described using the transverse coordinate x. However, in the state of large deformation, the actual axial coordinates of the beam will deviate, resulting in a deviation between the theoretical model based on the initial coordinates and the actual deformed configuration. To overcome this limitation, this article uses arc coordinates to characterize the position and deformation of the structure, assuming that the beam structure is inextensible and the material is isotropic and linear elastic. The schematic diagram of a bending cantilever beam in the arc length coordinate is shown in Figure 1.

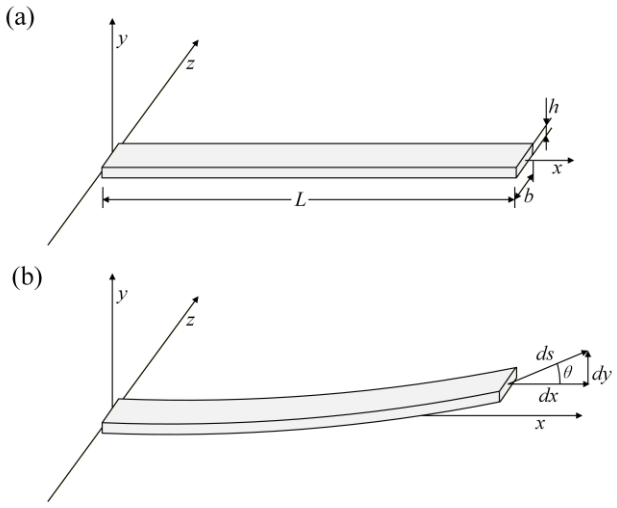


Figure 1 – Deflection diagram of a cantilever beam in arc length coordinate: (a)undeformed, (b)deformed.

The position coordinates of the cantilever at position $s=s_0$ can be expressed as following:

$$x(s_0,t)=\int_0^{s_0}\cos\theta(s,t)\,ds,\quad y(s_0,t)=\int_0^{s_0}\sin\theta(s,t)\,ds \tag{1}$$

The velocities can be written as:

$$v_x(s_0,t)=\int_0^{s_0}\left[-\sin\theta(s,t)\frac{\partial\theta(s,t)}{\partial t}\right]ds,\quad v_y(s_0,t)=\int_0^{s_0}\left[\cos\theta(s,t)\frac{\partial\theta(s,t)}{\partial t}\right]ds \tag{2}$$

Where $\theta(s, t)$ is the rotation angle of cross-section at arc length coordinate s. The rotation angle can be written by the Galerkin method as follows:

$$\theta(s,t)=\sum_{i=1}^{N}\varphi_i(s)q_i(t) \tag{3}$$

For the cantilever beam, the shape function of $\varphi_i(s)$ is:

$$\varphi_i(s)=\beta_i\left\{\sinh(\beta_i s)+\sin(\beta_i s)-\alpha_i\left[\cosh(\beta_i s)-\cos(\beta_i s)\right]\right\} \tag{4}$$

where α_i and β_i satisfy:

$$\alpha_i=\frac{\cosh(\beta_i L)+\cos(\beta_i L)}{\sinh(\beta_i L)+\sin(\beta_i L)} \tag{5}$$

$$1+\cos(\beta_i L)\cosh(\beta_i L)=0 \tag{6}$$

Due to the beam is inextensible, the bending strain energy of the structure is only caused by curvature κ. The bending strain energy of a cantilever beam can be expressed in curvature:

$$U_b=\frac{EI}{2}\int_0^L\kappa^2 ds=\frac{EI}{2}\int_0^L\left(\frac{d\theta}{ds}\right)^2 ds=\frac{EI}{2}\int_0^L\left(\sum_{i=1}^{N}\varphi_i'(s)q_i(t)\right)^2 ds \tag{7}$$

where E is the elastic modulus, I is the moment of inertia of the cross-section per unit length, and L is the length of the cantilever beam.

The translational terms and rotational terms of the kinetic energy can be written as:

$$T_{\text{trans}}=\frac{1}{2}\int_0^L\rho\left(v_x{}^2+v_y{}^2\right)ds \tag{8}$$

$$T_{\text{rot}}=\frac{1}{2}\int_0^L J\left(\frac{\partial\theta(s,t)}{\partial t}\right)^2 ds \tag{9}$$

where ρ is the mass per unit length of the cantilever, J is the moment of inertia of the section and $J=\rho h^2/12$ for a unit length rectangular section.

Assuming the external force F_x (positive to the right), the external force F_y (positive upwards), and the torque M (positive counterclockwise) are all acting at the arc length coordinate $s=s_0$, and gravity g acts in the constant negative y-axis direction, the virtual work can be written as:

$$\delta W_F=-F_x\int_0^{s_0}\sin\left[\theta(s,t)\right]\delta\theta ds+F_y\int_0^{s_0}\cos\left[\theta(s,t)\right]\delta\theta ds \tag{10}$$

$$\delta W_M=M\,\delta\theta(s_0,t) \tag{11}$$

$$\delta W_g=-\rho g\int_0^L(L-s)\cos\theta(s,t)\,\delta\theta ds \tag{12}$$

By substituting potential energy, kinetic energy, and virtual work into the Lagrange equation, and taking partial derivatives with respect to the generalized coordinates q_r the following results can be obtained:

$$\sum_j^N M_{rj}(\mathbf{q})\ddot{q}_j+\sum_i^N\sum_j^N C_{r,ij}(\mathbf{q})\dot{q}_i\dot{q}_j+\sum_j^N K_{rj}(\mathbf{q})\ddot{q}_j=Q_{F_r}+Q_{M_r}+Q_{g_r},\quad r=1,\ldots,N \tag{13}$$

where M is the inertial matrix, $C_{r,ij}$ is the Christoffel symbol term[34, 35], K is the stiffness matrix, Q_F, Q_M and Q_g are the generalized forces corresponding to the external force, external torque, and gravity, respectively. These terms can be written as:

Assuming the damping form of the system is linear modal damping, that is:

$$\sum_{j}^{N} M_{rj}(\mathbf{q})\ddot{q}_j + \sum_{j}^{N} 2\xi M_{0,rj}\omega_j \dot{q}_j + \sum_{i}^{N}\sum_{j}^{N} C_{r,ij}(\mathbf{q})\dot{q}_i\dot{q}_j + \sum_{j}^{N} K_{rj}(\mathbf{q})\ddot{q}_j = Q_{F_r} + Q_{M_r} + Q_{g_r} \tag{14}$$

where ξ is the damping ratio, ω_j are the linear natural frequencies of each mode, and M_0 is the inertial matrix in an undeformed state.

2.2 Modal analysis

To characterize the system dynamics and validate the present approach, we can conduct linear modal analysis for the undeformed structure, and prestressed modal analysis for the beam structure undergoing large deformation, based on the established governing equations.

The system inertial matrix is defined as $\mathbf{M}_{\mathrm{L}}$ and the stiffness matrix is defined as $\mathbf{K}_{\mathrm{L}}$ in the undeformed state. The natural frequency of the linear structure satisfies:

$$\left(\mathbf{K}_{\mathrm{L}} - \omega_{\mathrm{L}}^2 \mathbf{M}_{\mathrm{L}}\right)\boldsymbol{\Phi} = 0 \tag{15}$$

where $\boldsymbol{\Phi}$ represents the system eigenvector, i.e. the mode shape.

Assuming the static equilibrium position of the beam under external force is $\mathbf{q}_0$, and the tangent inertia matrix $\mathbf{M}_{\mathrm{NL}}$ and tangent stiffness matrix $\mathbf{K}_{\mathrm{NL}}$ in this state are:

$$\mathbf{M}_{\mathrm{NL}} = \mathbf{M}(\mathbf{q}_0) \tag{16}$$

$$\begin{aligned}\mathbf{K}_{\mathrm{NL}} &= \frac{\partial}{\partial q_h}\left(\frac{\partial U_b}{\partial q_r} - Q_F - Q_M - Q_g\right)\Bigg|_{\mathbf{q}=\mathbf{q}_0} \\ &= \mathbf{K}_b + \mathbf{K}_F(\mathbf{q}_0) + \mathbf{K}_M + \mathbf{K}_g(\mathbf{q}_0)\end{aligned} \tag{17}$$

where:

$$K_{F_{rh}} = F_x \int_0^{s_0} \varphi_r(s)\varphi_h(s)\cos\left(\sum_{k=1}^{N}\varphi_k(s)q_{0_k}\right)ds + F_y \int_0^{s_0} \varphi_r(s)\varphi_h(s)\sin\left(\sum_{k=1}^{N}\varphi_k(s)q_{0_k}\right)ds \tag{18}$$

$$K_{M_{rh}} = -\frac{\partial\left[M\varphi_r(s_0)\right]}{\partial q_h} = 0 \tag{19}$$

$$K_{g_{rh}} = -\rho g \int_0^{L} (L-s)\varphi_r(s)\varphi_h(s)\sin\left(\sum_{k=1}^{N}\varphi_k(s)q_{0_k}\right)ds \tag{20}$$

Therefore, the linearized natural frequency of the prestressed structure undergoing large deflection satisfies:

$$\left(\mathbf{K}_{\mathrm{NL}} - \omega_{\mathrm{NL}}^2 \mathbf{M}_{\mathrm{NL}}\right)\boldsymbol{\phi} = 0 \tag{21}$$

By solving the eigenvalue problem, linearized natural frequency ω_{NL} of the prestressed structure can be obtained.

3. Result and Discussion

3.1 Comparison of static deflection

To validate the present theory, the beam model from Ref. [37] is selected. The length L, width b, and thickness h of the cantilever beam is defined as 0.508 m, 0.0285496 m, and 0.001778 m, respectively. The material is aluminum, with an elastic modulus of 69.3 GPa and a density of 2840 kg/m^3. In the analysis, gravitational effects are neglected, and a concentrated load ranging from 0 to 0.815 kg is applied at the tip of the cantilever beam. The static deformations undergoing various external loads are obtained by solving the governing equation. The deformation is normalized by the beam length L. The results obtained from the present theoretical model are compared with experimental data from Dowell et al. [37, 38], numerical simulations, and the solution of the inextensible beam theory. The comparison is presented in Figure 2.

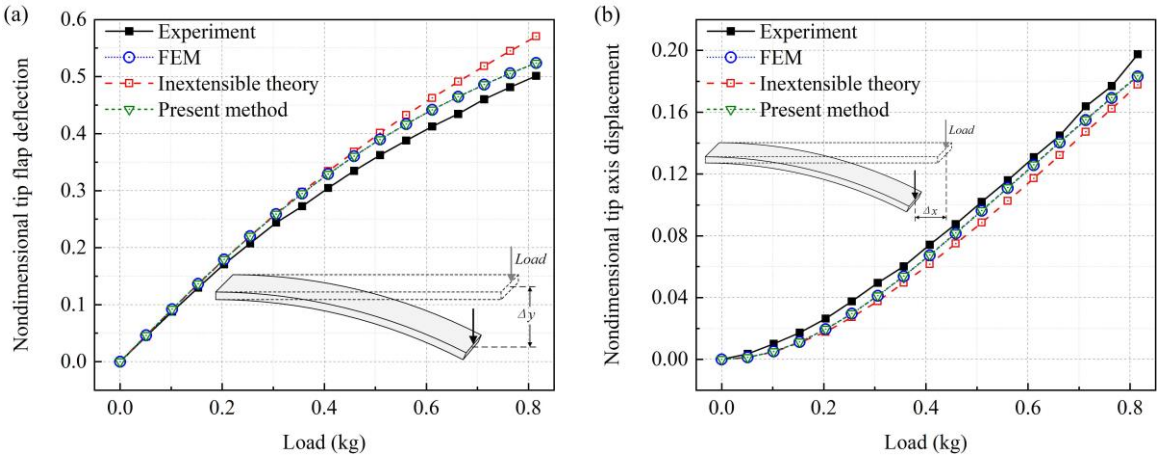


Figure 2 – Nondimensional (a) tip flap deflection and (b) tip axial displacement of a cantilever beam as a function of the load applied at the tip.

As the concentrated load increases, the deformation of the free end of the cantilever beam gradually increases. Due to the influence of geometric nonlinear effects, the increase in structural deformation gradually slows down, and the nonlinear effects become more significant. There are certain discrepancies between experimental and FEM results, which mainly comes from the processing method of experimental data. During the experiment, the measured deformation is the actual deformation of the structure minus the initial deformation caused by gravity. Gravitational loading amplifies the geometric nonlinearity of the structure, leading to slightly lower static deformation values in the experimental results compared to the simulation.

Comparing the present theoretical with FEM results and inextensible beam theoretical results, it can be concluded that the present theoretical predictions are in close agreement with the FEM results, whereas the inextensible beam theory yields certain deviations from the numerical simulations. This is because inextensible beams theory uses lateral coordinates to describe the position of load application, resulting in a deviation between the load position in the theoretical model and the actual position after structural deformation, thereby affecting the accuracy of theoretical calculations.

3.2 Comparison of linear and prestressed mode

Modal analyses were conducted for both the undeformed and deformed configurations of the structure. The load applied at the tip for the latter case is 0.815 kg. The modal frequencies are shown in Table 1 and the first three bending modal shapes of the deformed cantilever beam are shown in Figure 3. The present theoretical results show excellent agreement with those from Nastran simulations, validating the correctness of the present modal analysis framework. When subjected to an external load, the first nonlinear bending natural frequency increases compared to its linear counterpart. In contrast, the higher-order nonlinear modal frequencies decrease to varying degrees. As the modal order increases, the bending modal frequency of the structure gradually decreases under the influence of the load.

Table 1 – Modal frequencies calculated by numerical simulation and theoretical analysis.

Linear Modal ω_L (Hz)			Prestressed Modal ω_{NL} (Hz)			$\Delta\omega/\omega_{linear}$
Nastran	Present method	Relative error	Nastran	Present method	Relative error	
5.498	5.499	0.014%	6.865	6.865	0.013%	24.86%
34.454	34.465	0.032%	33.388	33.407	0.057%	-3.07%
96.486	96.573	0.090%	91.549	91.566	0.019%	-5.18%
189.009	189.468	0.243%	184.051	184.231	0.098%	-2.76%
312.412	313.555	0.366%	307.289	307.421	0.043%	-1.96%
466.633	469.390	0.591%	462.266	463.173	0.196%	-1.32%
651.667	656.895	0.802%	649.590	650.469	0.135%	-0.98%

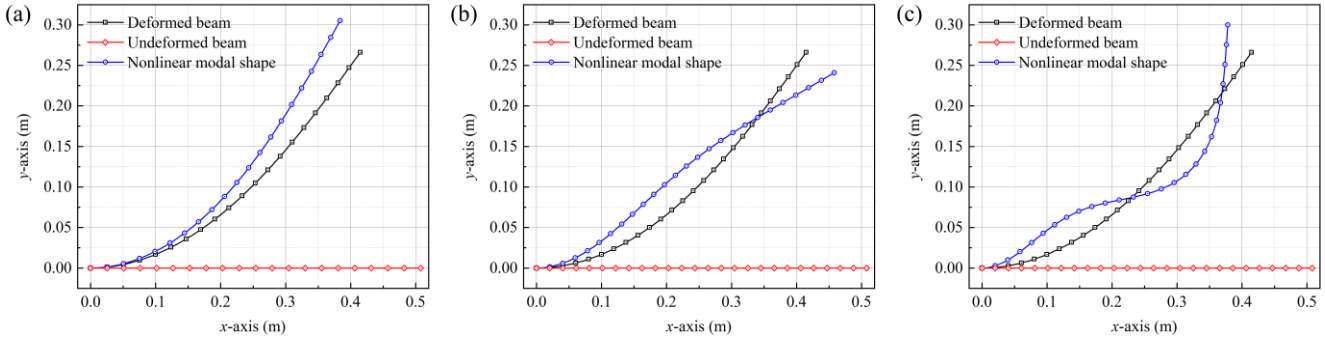


Figure 3 – The first three modal shapes of a deformed cantilever beam

3.3 Comparison of dynamic response

To verify the accuracy of the presented theoretical model for dynamic response, a sinusoidal excitation along the y-direction was applied to the free end of the cantilever beam, with the forcing function given by F_y=3sin(10t). The x-direction excitation force F_x, torque M, and gravitational acceleration g are all set to 0, and the damping ratio ξ is set to 0. By solving the governing equations via the Newmark-β method, the undamped dynamic response undergoing the sinusoidal excitation was obtained. For the theoretical model, the total simulation time was set to 4 s with a time step of 0.0025 s. Compare the present theoretical model with the Nastran calculation results, as shown in Figure 4, demonstrating that the results from the present model are in quite good agreement with the numerical simulations.

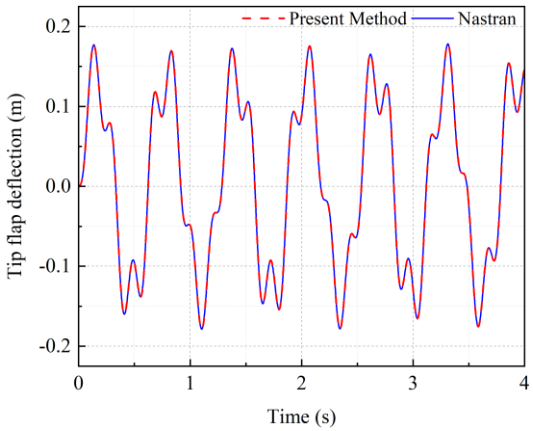


Figure 4 – Nondimensional (a) tip flap deflection and (b) tip axial displacement of a cantilever beam as a function of the load applied at the tip.

The dynamic characteristics of the structure were tested using the sine sweep excitation method. y-direction sine excitation forces with an amplitude of 0.25 N were applied to the tip of the cantilever beam. The excitation frequency range was 5 Hz to 6 Hz, and the frequency resolution was 0.025 Hz. The excitation duration at each frequency point was 40 seconds. After the excitation at each frequency was completed, the instantaneous response state of the structure was used as the initial condition for the next frequency excitation. The damping ratio ξ is set to 0.005. Forward and reverse frequency sweeps were both performed. Figure 5 shows the steady-state response at each frequency for the forward sweep and backward sweep, with both responses taken from the last 0.5 seconds of the excitation signal.

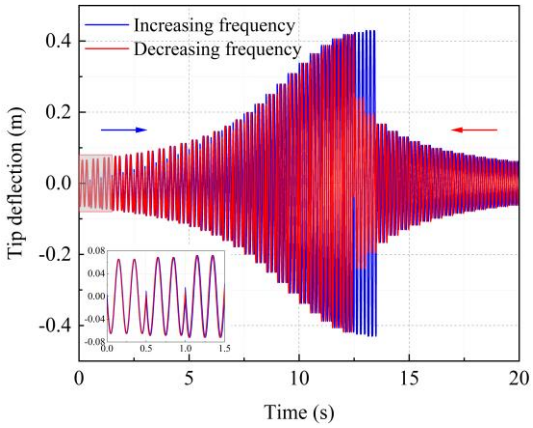


Figure 5 – The steady-state response for increasing and decreasing excitation frequency

As the excitation frequency gradually toward the first linear frequency, the amplitude of the sweep frequency response curves gradually increases, but with a sudden drop at different frequencies for the forward and backward sweeps.

To further investigate the influence of excitation force amplitude, sine sweeps were carried out at four different force levels: 0.1 N, 0.15 N, 0.2 N, and 0.25 N. Extract the steady-state response of each frequency point for the last 3 seconds and perform FFT to obtain the frequency response curve. Then, the amplitude peak and its corresponding frequency are extracted as shown in Figure 6, where the black dashed line corresponds to the first linear mode frequency.

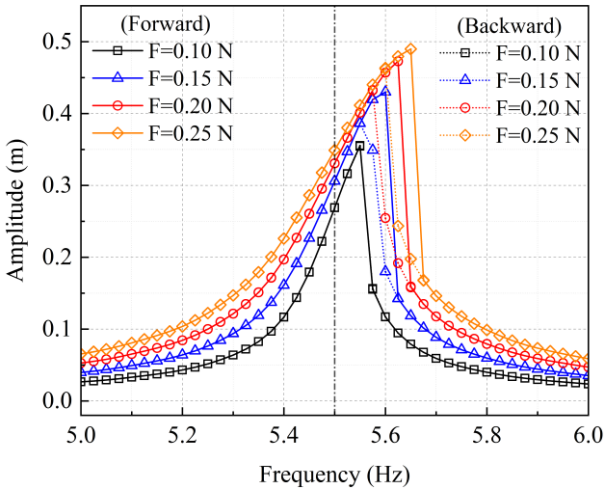


Figure 6 – The frequency response characteristics with different excitation amplitude

When the amplitude of sine excitation is 0.1 N, the forward sweep curve and reverse sweep curve completely overlap, indicating that the system's dynamic response is independent of the sweep path. Due to the given damping being linear damping, the energy dissipation in this small amplitude vibration state is proportional to the velocity, and geometric nonlinear effects do not introduce additional energy dissipation. The structural recovery force and displacement exhibit a linear relationship, resulting in a response that exhibits linear characteristics.

According to Figure 6, as the excitation force increases, the amplitude of the structural response gradually increases. When the amplitude of dynamic response approaches the beam length, the change in the structural dynamic response with the increase of excitation force is not significant. The structural deformation reaches saturation, and the external input energy is dissipated by the nonlinear characteristics of the structure. Simultaneously, the first mode exhibits stiffness hardening phenomenon, and the structural resonance frequency shifts to the right. Consequently, there is a difference in the frequency response characteristics obtained from the forward and reverse sweep of the system, and the frequency response curve shows hysteresis characteristics, indicating that the system exhibits nonlinear characteristics. This is because the mass matrix and stiffness matrix of the cantilever beam are functions of the configuration. When the structure undergoes large

deformation or rotation, the internal stiffness will undergo significant changes with the deformation state, causing the dynamic characteristics of the system to change with the motion state.

Nonlinear systems possess multiple steady states near the resonance region. The sweep path affects the initial conditions of the system, thereby determining its convergence toward the nearest steady state. When performing forward sweep, the response amplitude gradually increases with frequency, and the stiffness hardening phenomenon of the first mode causes the corresponding resonance frequency to gradually increase. When the frequency increases to a critical value, the dynamic equilibrium state of the system undergoes a sudden change, and the response amplitude drops sharply to a lower level. When performing reverse frequency sweep, the system begins to vibrate from a high-frequency state. When the frequency decreases to the vicinity of the resonance zone, due to the different loading paths, the equivalent stiffness change path of the system differs from the forward sweep frequency, causing the response amplitude to gradually increase along another path and jump at another critical point. Due to the different evolution paths of system stiffness during forward and reverse frequency sweep processes, the critical points corresponding to jumps are different, and the frequency response curve exhibits hysteresis.

4. Conclusions

In this study, the geometrically exact inextensible beam model based on arc-length coordinates and rotation angle has been established using the Galerkin approach without any simplification. Through comprehensive comparisons with finite element simulations, classical analytical solutions, and experimental data, the present model demonstrates high accuracy in predicting static deformation, linear modal frequencies, prestressed modal characteristics, and dynamic responses. The typical nonlinear characteristics can be captured by present theoretical model, such as stiffness hardening, softening, and hysteresis phenomena.

5. Contact Author Email Address

mailto: guyingsong@nwpu.edu.cn

6. Copyright Statement

The authors confirm that they, and/or their company or organization, hold copyright on all of the original material included in this paper. The authors also confirm that they have obtained permission, from the copyright holder of any third party material included in this paper, to publish it as part of their paper. The authors confirm that they give permission, or have obtained permission from the copyright holder of this paper, for the publication and distribution of this paper as part of the ICAS proceedings or as individual off-prints from the proceedings.

References

[1] Reissner E. On one-dimensional finite strain beam theory: The plane problem. Zeitschrift für angewandte Mathematik und Physik ZAMP. Vol. 23, No. 5, pp 795-804, 1972.

[2] Reissner, E. On One‐Dimensional Large‐Displacement Finite‐Strain Beam Theory. Studies in Applied Mathematics. Vol. 52, No. 2, pp 87-95, 1973.

[3] Reissner E. On finite deformations of space-curved beams. Zeitschrift für angewandte Mathematik und Physik ZAMP. Vol. 32, No. 6, pp 734-744, 1981.

[4] Simo J C, Vu-Quoc L. On the dynamics in space of rods undergoing large motions—a geometrically exact approach. Computer methods in applied mechanics and engineering. Vol. 66, No. 2, pp 125-161, 1988.

[5] Simo J C, Vu-Quoc L. A three-dimensional finite-strain rod model. Part II: Computational aspects. Computer methods in applied mechanics and engineering. Vol. 58, No. 1, pp 79-116, 1986.

[6] Simo J C. A finite strain beam formulation. The three-dimensional dynamic problem. Part I. Computer methods in applied mechanics and engineering. Vol. 49, No. 1, pp 55-70, 1985.

[7] Ghosh S, Roy D. A frame-invariant scheme for the geometrically exact beam using rotation vector parametrization. Computational Mechanics. Vol. 44, No. 1, pp 103-118, 2009.

[8] Herath S, Yin G. On the geometrically exact formulations of finite deformable isogeometric beams. Computational Mechanics. Vol. 67, No. 6, pp 1705-1717, 2021.

[9] Culver D, McHugh K, Dowell E. An assessment and extension of geometrically nonlinear beam theories. Mechanical Systems and Signal Processing. Vol. 134, No. pp 106340, 2019.

[10] Su W. Coupled Nonlinear Aeroelasticity and Flight Dynamics of Fully Flexible Aircraft[D]: University of

Michigan, 2008.

[11]Su W, Cesnik C E. Strain-based geometrically nonlinear beam formulation for modeling very flexible aircraft. International Journal of Solids and Structures. Vol. 48, No. 16-17, pp 2349-2360, 2011.

[12]Pang Z Y, Cesnik C E S, editors. Strain state estimation of very flexible unmanned aerial vehicle. 57th AIAA/ASCE/AHS/ASC Structures, Structural Dynamics, and Materials Conference; 2016. San Diego, CA, U.S.AJanuary, 2016.

[13]Chang C-S, Hodges D H, editors. Modeling of ground vibration testing for highly flexible aircraft. 47th AIAA/ASME/ASCE/AHS/ASC Structures, Structural Dynamics, and Materials Conference; 2006. Newport, Rhode IslandMay, 2006.

[14]Sari Ma'en S. Nonlinear forced response of non-uniform beams carrying point masses using the harmonic balance method with an arc-length continuation scheme. Advances in Mechanical Engineering. Vol. 17, No. 2, pp 1-13, 2025.

[15]Wang Y, Zhu W. Nonlinear transverse vibration of a hyperelastic beam under harmonic axial loading in the subcritical buckling regime. Applied Mathematical Modelling. Vol. 94, No. pp 597-618, 2021.

[16]Qian Y H, Pan J L, Chen S P, Yao M H. The Spreading Residue Harmonic Balance Method for Strongly Nonlinear Vibrations of a Restrained Cantilever Beam. Advances in Mathematical Physics. Vol. 2017, No. pp 1-8, 2017.

[17]Guo Z, Zhang W. The spreading residue harmonic balance study on the vibration frequencies of tapered beams. Applied Mathematical Modelling. Vol. 40, No. 15, pp 7195-7203, 2016.

[18]Bennett J A, Eisley J G. A multiple degree-of-freedom approach to nonlinear beam vibrations. AIAA Journal. Vol. 8, No. 4, pp 734-739, 1970.

[19]Hodges D, Dowell E H. Nonlinear equations of motion for the elastic bending and torsion of twisted nonuniform rotor blades. NASA TN. Vol. No. pp D-7818, 1975.

[20]Dowell E, Traybar J, Hodges D H. An experimental-theoretical correlation study of non-linear bending and torsion deformations of a cantilever beam. Journal of Sound and Vibration. Vol. 50, No. 4, pp 533-544, 1977.

[21]Hodges D H. Proper definition of curvature in nonlinear beam kinematics. AIAA journal. Vol. 22, No. 12, pp 1825-1827, 1984.

[22]Tang D M, Dowell E H. Effects of geometric structural nonlinearity on flutter and limit cycle oscillations of high-aspect-ratio wings. Journal of Fluids and Structures. Vol. 19, No. 3, pp 291-306, 2004.

[23]Liu W H, Kou H S, Yang F S. Non-linear vibrations of beams with elastically restrained edges. Journal of Sound and Vibration. Vol. 121, No. 2, pp 375-381, 1988.

[24]Weiliang Y, Dowell E. Limit cycle oscillation of a fluttering cantilever plate. AIAA Journal. Vol. 29, No. 11, pp 1929-1936, 1991.

[25]Firouzi N, Alzaidi A S, Nezaminia H, Dalalchi D. Numerical investigation on effect of different parameters on nonlinear vibration response of fully geometrically exact Timoshenko beams. Applied Physics A. Vol. 130, No. 9, pp 618, 2024.

[26]Kimiaeifar A, Tolou N, Barari A, Herder J. Large deflection analysis of cantilever beam under end point and distributed loads. Journal of the Chinese Institute of Engineers. Vol. 37, No. pp 438–445, 2014.

[27]Bhashyam G, Prathap G. Galerkin finite element method for non-linear beam vibrations. Journal of sound and vibration. Vol. 72, No. 2, pp 191-203, 1980.

[28]Sfahani M, Barari A, Omidvar M, Ganji S, Domairry G. Dynamic response of inextensible beams by improved energy balance method. Proceedings of the Institution of Mechanical Engineers, Part K: Journal of Multi-body Dynamics. Vol. 225, No. 1, pp 66-73, 2011.

[29]Deliyianni M, Gudibanda V, Howell J, Webster J T. Large deflections of inextensible cantilevers: modeling, theory, and simulation. Mathematical Modelling of Natural Phenomena. Vol. 15, No. pp 44, 2020.

[30]Deliyianni M, McHugh K, Webster J T, Dowell E. Dynamic equations of motion for inextensible beams and plates. Archive of Applied Mechanics. Vol. 92, No. 6, pp 1929-1952, 2022.

[31]Lacarbonara W, Yabuno H. Refined models of elastic beams undergoing large in-plane motions: Theory and experiment. International Journal of Solids and Structures. Vol. 43, No. 17, pp 5066-5084, 2006.

[32]Fiori S. Variational formulation of a fully-three-dimensional non-linear beam dynamics by a Lie-group representation. AIMS Mathematics. Vol. 10, No. 9, pp 21953-21993, 2025.

[33]Luongo A, D'Annibale F. Nonlinear hysteretic damping effects on the post-critical behaviour of the visco-elastic Beck's beam. Mathematics and Mechanics of Solids. Vol. 22, No. 6, pp 1347-1365, 2017.

[34]Sheinman I. Dynamic large-displacement analysis of curved beams involving shear deformation. International Journal of Solids and Structures. Vol. 16, No. 11, pp 1037-1049, 1980.

[35]Echeandia S, Wensing P M. Numerical methods to compute the coriolis matrix and christoffel symbols

for rigid-body systems. Journal of Computational and Nonlinear Dynamics. Vol. 16, No. 9, pp 091004, 2021.

[36] Hoskoti L, Sucheendran M M, editors. Nonlinear Vibration of an Inextensible Rotating Beam. Advances in Nonlinear Dynamics, Volume I; 2024 2024//; Cham: Springer Nature Switzerland.

[37] Tang D, Zhao M, Dowell E H. Inextensible beam and plate theory: computational analysis and comparison with experiment. Journal of Applied Mechanics-Transactions of the Asme. Vol. 81, No. 6, pp 061009, 2014.

[38] McHugh K, Dowell E. Nonlinear responses of inextensible cantilever and free-free beams undergoing large deflections. Journal of Applied Mechanics-Transactions of the Asme. Vol. 85, No. 5, pp 051008, 2018.